ISBN: 978-3-95450-249-3 ISSN: 2673-5350 doi: 10.18429/JACoW-IBIC2024-TUP16

DEVELOPMENT STATUS OF THE BPM SYSTEM FOR THE SPring-8-II STORAGE RING

H. Maesaka*, [1], RIKEN SPring-8 Center, Sayo, Hyogo, Japan
H. Dewa, T. Fujita, M. Masaki, S. Suzuki, S. Takano[2], JASRI, Sayo, Hyogo, Japan
[1]also at JASRI, Sayo, Hyogo, Japan
[2]also at RIKEN SPring-8 Center, Sayo Hyogo, Japan

Abstract

We have developed a button-type BPM system for the fourth-generation light source, SPring-8-II, which is the low-emittance upgrade of SPring-8. In total, 340 BPMs will be fabricated and installed into SPring-8-II. The BPM prototype has been tested in present SPring-8 and almost the same BPM system was installed into the new 3 GeV light source, NanoTerasu. The design of the BPM head for SPring-8-II was recently modified, since the cross-section of the beam pipe was redesigned. BPM signals are transmitted to the readout electronics by radiation-resistant coaxial cables and processed by MicroTCA.4-based electronics. We evaluated the beam position sensitivity, impedance, thermal structure issues, position resolution, long-term stability, and electrical center displacement. The single-pass resolution was less than 100 μm std. for a 0.1 nC injected bunch and the COD resolution was less than 1 μm std. for a wide range of stored current. The long-term stability was within 5 μm for several weeks. The displacement of the electrical center is less than 150 μm std. These results are sufficient for the commissioning and operation of SPring-8-II.

INTRODUCTION

The construction of the fourth-generation light source, SPring-8-II [1–3], is being started, which is the low-emittance upgrade of the third-generation light source, SPring-8. The beam energy will be decreased from 8 GeV to 6 GeV and the lattice structure will be changed from double-bend achromat to five-bend achromat. As a result, the natural emittance will be improved from 2.4 nm rad to 100 pm rad or less and the X-ray brilliance around 10 keV will be increased by about 100 times.

To utilize brilliant X-rays effectively, the electron beam orbit should be monitored precisely and stably and the X-ray optical axis should be stabilized as much as possible. The stability of the beam orbit is required to be within 5 μm for one month. Furthermore, it is indicated that there is no stable closed orbit at the commissioning stage due to the strong quadrupole and sextupole magnets with finite alignment errors. Therefore, the single-pass beam trajectory must be precisely measured by the BPM system and the beam must be steered carefully until a stable closed orbit is found, so-called first-turn steering (FTS). Requirements for the FTS are a precise single-pass resolution of 100 μm std. for a 0.1 nC injected bunch and a small electric and mechanical center error within 200 μm.

We have developed a new button-type BPM system for SPring-8-II, which fulfills the above requirements. Almost the same BPM system was employed for a new 3 GeV light source, NanoTerasu [4–8], and it has been working stably in commissioning and user services. A part of the BPM readout electronics in SPring-8 was replaced with the new system [9] for the adaptive feedforward correction of fast helicity-switching beamlines [10] and the renewal of the old single-pass BPM system [11]. Based on these experiences, we are improving the BPM system design.

In this article, we describe an overview of the BPM system for SPring-8-II, the development status, and evaluated basic performances.

BPM SYSTEM

We employed a button-type BPM for SPring-8-II, which is common for many electron storage rings. In this section, we describe the BPM layout, the BPM head design, BPM support, signal cables, and readout electronics.

BPM Layout

The SPring-8-II storage ring has a total of 48 unit cells, consisting of 44 five-bend cells and 4 long-straight cells. Each five-bend cell has 7 BPMs and each long-straight cell has 8 BPMs, as shown in Fig. 1 together with the magnet arrangement. Thus, 340 BPMs in total will be fabricated and installed.

BPM Head

The cross-section of the beam pipe was originally designed as a squeezed octagonal shape [1, 12, 13] and this design was employed for NanoTerasu [4, 14]. The beam pipe has then been changed to a rhombus shape to reduce the resistive-wall impedance [15]. Since the original beam pipe made of stainless steel has a larger resistive-wall impedance than the new one, copper plating on the inner surface is necessary. However, the new beam pipe has a sufficiently small impedance even if it is made of stainless steel without copper plating.

Therefore, the design of the BPM head has also been modified to fit the new beam pipe, as shown in Fig. 2. The button electrode itself has not been changed from the original design [16]. The diameter of the electrode is 7 mm and that of the hole for the electrode is 8 mm. Therefore, the gap around the electrode is 0.5 mm. The distance from the

* maesaka@spring8.or.jp

ISBN: 978-3-95450-249-3 ISSN: 2673-5350 doi: 10.18429/JACoW-IBIC2024-TUP16

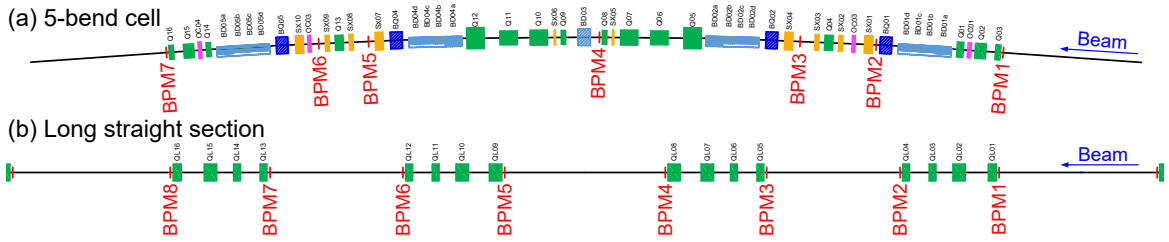

Figure 1: Layout of BPMs and magnets for the 5-bend cell (a) and the long straight section (b). BPMs are shown by red lines. Dipoles, dipole-quadrupole combined magnets, quadrupoles, sextupoles, and octupoles are illustrated by cyan, blue, green, orange, and magenta boxes, respectively.

beam axis to each electrode is 13.06 mm and the electrode is located at the center of each side of the rhombus.

The materials of the electrode and the BPM block are molybdenum and stainless steel, respectively. Since molybdenum has better electrical conductivity than stainless steel, most of the electromagnetic heating in the BPM occurs on the stainless steel side and the temperature rise of the electrode can be relaxed. The BPM block has a water-cooling channel upstream or downstream of the electrodes to suppress the temperature rise and the thermal deformation.

The beam signal from each electrode is extracted from a reverse-polarity (RP) SMA receptacle and transmitted to readout electronics by a coaxial cable. By using RP-SMA connectors, any spring materials in the electrode are eliminated and troubles in the connector part of the electrode can be prevented.

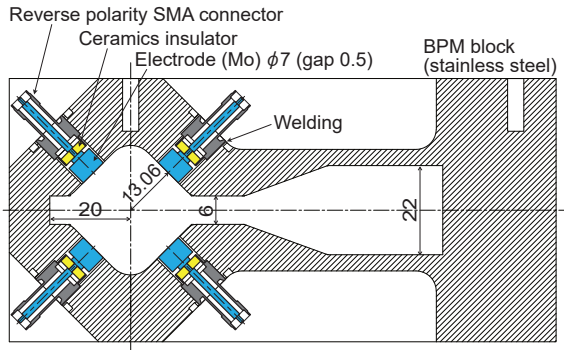

Figure 2: Schematic cross-sectional view of the BPM head. The unit of dimensions is mm.

BPM Support

Since BPMs 3, 5, and 6 in the five-bend cell are supported by vacuum chambers for X-ray absorbers, BPM supports are not needed. Thus, we designed BPM supports for BPMs 1, 2, 4, and 7. A typical support structure is shown in Fig. 3. This support is mounted on the common girder with other magnets and vacuum chambers. The distance between the top of the common girder to the beam axis is 400 mm. This support has an adjustment function of the position and angle of the BPM and also has enough strength for the BPM to be a fixed point. The stresses on the BPM are supposed to be 100 N for horizontal and 400 N for vertical. We analyzed the deformation of the support under these stresses and the displacement of the BPM was less than 30 µm for both horizontal and vertical directions. Since the stress does not vary during a stable operation condition, this displacement is sufficiently small for our application.

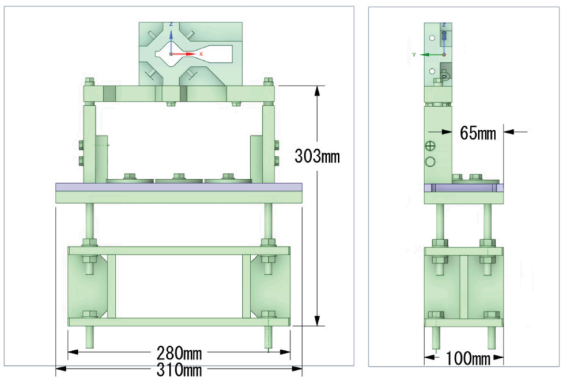

Figure 3: Schematic drawing of the BPM support.

Signal Cables

Important characteristics of BPM signal cables are small insertion loss, large return loss, and radiation resistance for stable and precise beam position measurement. In fact, radiation-damaged cables in SPring-8 became sensitive to humidity and the BPM data showed a correlation with humidity [17]. Therefore, radiation resistivity is quite important for a cable in a radiation environment. Consequently, we use three types of coaxial cables, A-, B-, and C-cables, depending on the radiation condition, flexibility, and RF characteristics. This combination of the cables is already used in NanoTerasu [5] and the handling and the performance of the cables have been established.

The A-cable is attached to the BPM head and connected to the B-cable beside the girder. Since the radiation dose is the highest around the A-cable, We put several kinds of cables in a radiation environment in the SPring-8 storage ring and investigated the radiation resistivity [18]. We then employed a PEEK-insulated semi-rigid cable as an A-cable, which is highly radiation-resistive and has relatively reasonable price. Although the PEEK cable has relatively higher insertion loss of 0.6 dB/m at 500 MHz, the length is only 1.5 m and the insertion loss can be acceptable.

ISBN: 978-3-95450-249-3 ISSN: 2673-5350 doi: 10.18429/JACoW-IBIC2024-TUP16

We selected a corrugated coaxial cable with a polyethylene insulator as a B-cable. This cable has a very small insertion loss of 0.06 dB/m at 500 MHz and relatively high radiation resistivity. Since the radiation dose is relatively small around the side of the girder, this B-cable is enough to prevent radiation damage. The B-cable transfers the BPM signal close to the readout electronics several 10 m apart from the BPM head.

Finally, the BPM signal is fed into the readout electronics by a C-cable. The C-cable is a standard flexible coaxial cable with a length of 2 m.

Readout Electronics

The readout electronics detect the signal intensity from each BPM electrode and calculate the beam position from the four BPM signals of a BPM. The electronics are also required to have both a COD (Closed Orbit Distortion) BPM mode with some different sampling rates and a single-pass (SP) BPM mode. Therefore, high-speed data processing and high data transfer rates are necessary. Thus, we employed MicroTCA.4 as a platform of the electronics and developed high-speed digitizer and RF frontend modules [9].

A schematic diagram of the readout electronics is shown in Fig. 4. The electronics are comprised of high-speed digitizer advanced mezzanine cards (AMC) and RF frontend rear transition modules (RTM). The BPM signal synchronized to the acceleration RF frequency of 508.76 MHz is extracted by a band-pass filter and the signal level is adjusted by step attenuators and amplifiers. The signal is converted to a balanced differential signal and digitized by a high-speed A/D converter with a sampling rate of 363.40 MHz, which is 5/7 of the RF frequency. Since the sampling rate is slower than the signal frequency, the signal is detected by an under-sampling scheme and the intermediate frequency of the obtained waveform is 145.36 MHz. This waveform is processed by a field-programmable gate array (FPGA) on the digitizer AMC and down-converted to an IQ (In-phase and Quadrature) baseband data.

The beam position is calculated from the four amplitude data of a BPM by 7th order polynomials of

$$\begin{aligned} D_x &= \frac{V_1 - V_2 - V_3 + V_4}{V_1 + V_2 + V_3 + V_4}, \\ D_y &= \frac{V_1 + V_2 - V_3 - V_4}{V_1 + V_2 + V_3 + V_4}, \\ \begin{pmatrix} X \\ Y \end{pmatrix} &= \sum_{n=0}^{7} \sum_{m=0}^{7-n} \begin{pmatrix} a_{nm} \\ b_{nm} \end{pmatrix} D_x^n D_y^m, \end{aligned} \tag{1}$$

where $V_1, \cdots, V_4$ are amplitudes of four BPM signals and a_{nm}, b_{nm} are conversion coefficients.

The COD-BPM part provides three data rates, 208.85 kHz turn-by-turn data, 10 kHz fast data, and 10 Hz slow data, in parallel. The SP-BPM part also calculates single-pass data at a turn-by-turn frequency of 208.85 kHz.

To stabilize the BPM data, the electronics are enclosed in a temperature-regulated water-cooled 19-inch cabinet to suppress temperature drifts. Furthermore, the RF frontend RTM has pilot tone generators and the drift of the gain of each channel can be monitored.

PERFORMANCE EVALUATION

Since the design of the BPM head was changed, we evaluated RF characteristics and performed a thermal structure analysis. To confirm the system performance, we experimentally obtained a position resolution, long-term stability, and electrical center error by using an electron beam.

RF Simulation

The three-dimensional RF simulation was conducted with CST Studio and the position sensitivity, trapped-mode heating, and beam impedance were analyzed.

The first-order coefficients of the BPM sensitivity (Eq. 1) were obtained to be 10.15 mm and 10.24 mm for horizontal and vertical directions, respectively. Although the sensitivity was decreased by about 30 % compared to the former design of the BPM head, the required position resolution was expected to be satisfied. On the other hand, the lower sensitivity relaxed the required machining accuracy by the same ratio. This result enables the fabrication of BPM heads easier.

The trapped-mode heating was evaluated with the bunch fill pattern of 406 × 0.5 mA, which is a relatively severe case among possible fill patterns. The bunch length was set to 14 ps std. considering the bunch lengthening due to longitudinal impedance. The result of the simulation showed that the heat input for each BPM was 1.7 W. The temperature rise is estimated to be small with this heat input when the BPM head is water-cooled.

The contribution to the beam impedance from the BPM head was also evaluated. The total impedance of all the BPM heads was estimated to be approximately 2 % of the total impedance from all the accelerator components for both transverse and longitudinal directions. This impedance value is small enough and no additional treatment to the BPM head is needed.

Thermal Structure Analysis

According to the heat input evaluated by the RF simulation, a thermal structure analysis was performed by using ANSYS [19]. The cooling water temperature and water flow were set to 30 °C and 4 L/min, respectively. In addition, water-cooled beam pipes were connected both upstream and downstream of the BPM head and a heat release to the air at 27 °C was also assumed.

If the BPM head is not water-cooled, the maximum temperature was estimated to be 44 °C, which was a temperature rise of more than 10 °C, and the displacement of the BPM head was found to be more than 10 µm. If the BPM head is water-cooled either upstream or downstream of the electrodes, the maximum temperature was suppressed to be 33 °C, and the displacement was to be less than 4 µm. From these results, we decided to equip the BPM head with a water-cooling channel.

ISBN: 978-3-95450-249-3 ISSN: 2673-5350 doi: 10.18429/JACoW-IBIC2024-TUP16

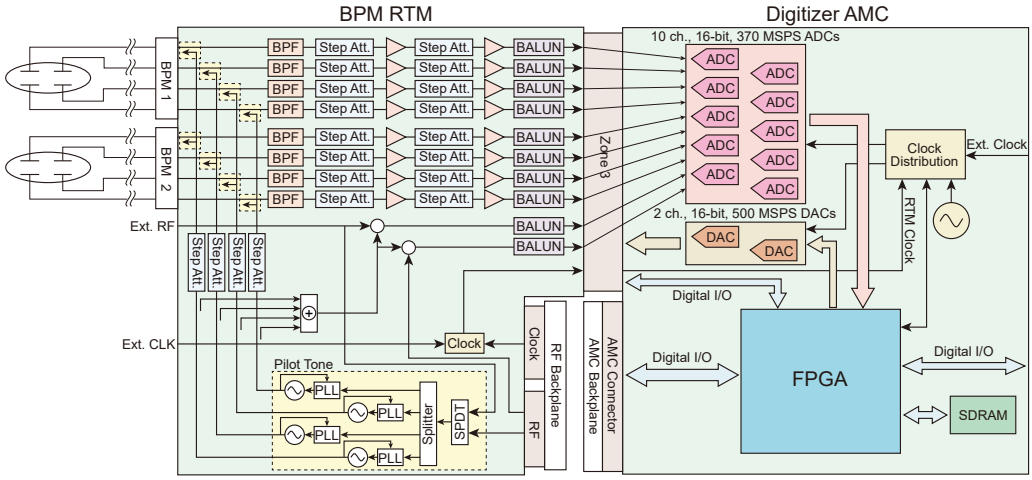

Figure 4: Block diagram of the BPM readout electronics.

Although these results were obtained from a simulation only, the reliability was considered to be sufficient. This is because we installed a similar BPM prototype into the SPring-8 storage ring and experimentally measured the temperature rise [18]. This measurement showed that the temperature was consistent with the simulation. Thus, the temperature measurement with the new BPM head is not needed.

Position Resolution

Although the position resolution was not measured by the new BPM head, the resolution is considered to be estimated from the result with another BPM head. We obtained the BPM data from the MicroTCA.4-based electronics with the present SPring-8 BPM head. The SP-BPM resolution in this case was evaluated to be 85 µm std. for a 0.1 nC injected bunch [11]. Since the new BPM head has higher sensitivity than the SPring-8 one, the resolution will be better than this result. The COD-BPM resolution was evaluated with another prototype BPM head and the result was 0.4 µm std. for 10 kHz fast data and a stored current of 30 mA [9]. Therefore, the new BPM system can measure COD with less than 1 µm resolution even if the stored current is not so large.

Long-term Stability

Long-term stability was evaluated with a BPM prototype installed into the present SPring-8 storage ring together with the MicroTCA.4-based electronics. When the temperature of the electronics was maintained within ± 0.1 °C, the drift of BPM reading was within 10 µm for 2 months. If the bunch fill pattern was not changed, the drift was within 5 µm for several weeks [9].

The temperature stability of a water-cooling 19-inch cabinet was also tested. If the ambient temperature was maintained within 1 °C and if the cooling water temperature was stabilized within 0.1 °C, the inside temperature was stable within ± 0.1 °C. Thus, the BPM system is considered to satisfy the stability requirement of 5 µm for 1 month.

Electrical Center Error

The electrical center error was evaluated with a prototype in SPring-8 and the BPMs for NanoTerasu. The prototype in SPring-8 has 4 BPMs in one block and the BPM data from the 4 BPMs are compared. The difference in the beam positions was within 100 µm [18]. In NanoTerasu, the displacement between the BPM center and the quadrupole magnetic center was measured by beam-based alignment. The standard deviation of the displacement was analyzed to be less than 150 µm [7, 8]. Thus, the required electrical center accuracy can be satisfied if we carefully fabricate, install, and test the BPM components.

SUMMARY AND PROSPECTS

We have developed the BPM system for SPring-8-II, consisting of 340 BPMs in total. Almost all the developed BPM components were employed by NanoTerasu and have been utilized for machine commissioning and user service. Since the cross-section of the beam pipe was redesigned recently, the BPM head was also modified according to the new cross-section without any serious problems. The radiation-resistant signal cables and the MicroTCA.4-based readout electronics are not changed from the original design for SPring-8-II. Various performances, such as RF characteristics, thermal structure property, position resolution, and long-term stability, are evaluated and all the results were confirmed to be sufficient.

From now on, we carefully and steadily proceed to the mass production of BPM components for SPring-8-II. The present SPring-8 will be shut down and dismantled in 2027 and the installation of SPring-8-II will then start. The commissioning of SPring-8-II is scheduled for late 2028.

REFERENCES

[1] "SPring-8-II Conceptual Design Report", Nov. 2014. http://rsc.riken.jp/pdf/SPring-8-II.pdf

[2] T. Watanabe and H. Tanaka, "SPring-8 upgrade project; accelerator redesigned and restarted", *Synchrotron Radiat. News*,

ISBN: 978-3-95450-249-3 ISSN: 2673-5350 doi: 10.18429/JACoW-IBIC2024-TUP16

vol. 36, pp. 3–6 (2023). doi://10.1080/08940886.2023.2186117

[3] H. Tanaka *et al.*, "Green Upgrading of SPring-8 to Produce Stable, Ultrabrilliant Hard X-ray Beams", *J. Synchrotron Radiat.*, to be published.

[4] "Accelerator design report for 3-GeV Next-Generation Synchrotron Radiation Facility", Sep. 2020. https://www.qst.go.jp/uploaded/attachment/18596.pdf

[5] H. Maesaka *et al.*, "Design of the Beam Diagnostic System for the New 3 GeV Light Source in Japan", in *Proc. 9th Int. Beam Instrumentation Conf. (IBIC'20)*, Santos (Online meeting), Brazil, Sep. 2020, pp. 174–178. doi://10.18429/JACoW-IBIC2020-WEPP31

[6] K. Ueshima *et al.*, "Status of beam commissioning at NanoTerasu", in *Proc. 15th Int. Particle Accelerator Conf. (IPAC'24)*, Nashville, TN, May 2024, pp. 1320–1323. doi://10.18429/JACoW-IPAC2024-TUPG40

[7] K. Ueshima *et al.*, "Commissioning of the Beam Diagnostic System for NanoTerasu: a new 3 GeV Light Source in Japan", presented at the 13th Int. Beam Instrumentation Conf. (IBIC'24), Beijing, China, Sep. 2024, TUBI1, this conference.

[8] S. Obara *et al.*, "Commissioning of a Compact Multi-Bend Achromat Lattice in NanoTerasu, a new 3 GeV Synchrotron Radiation Facility", submitted for publication.

[9] H. Maesaka *et al.*, "Development of MTCA.4-based BPM Electronics for SPring-8 Upgrade", in *Proc. 8th Int. Beam Instrumentation Conf. (IBIC'19)*, Malmö, Sweden, Sep. 2019, pp. 471–474. doi://10.18429/JACoW-IBIC2019-WEBO03

[10] M. Masaki *et al.*, "Adaptive feedforward control of closed orbit distortion caused by fast helicity-switching undulators", *J. Synchrotron Radiat.*, vol. 28, pp. 1758–1768, 2021. doi://10.1107/S160057752101047X

[11] H. Maesaka *et al.*, "Replacement of the Single-Pass BPM System with MicroTCA.4-based Versatile Electronics at SPring-8", in *Proc. 12th Int. Beam Instrumentation Conf. (IBIC'23)*, Saskatoon, Canada, Sep. 2023, pp. 74–77. doi:10.18429/JACoW-IBIC2023-MOP022

[12] M. Oishi *et al.*, "Design and R&D for the SPring-8 Upgrade Storage Ring Vacuum System", in *Proc. 7th Int. Particle Accelerator Conf. (IPAC'16)*, Busan, Korea, May 2016, pp. 3651–3653. doi://10.18429/JACoW-IPAC2016-THPMY001

[13] K. Tamura *et al.*, "Feasibility Tests of a Vacuum System for SPring-8-II", in *Proc. 10th Int. Particle Accelerator Conf. (IPAC'19)*, Melbourne, Australia, May 2019, pp. 1273–1275. doi://10.18429/JACoW-IPAC2019-TUPMP018

[14] K. Tamura *et al.*, "Storage Ring Vacuum System for 3-GeV Next-Generation Synchrotron Radiation Facility", in *Proc. 18th Annual Meeting of Particle Accelerator Society of Japan (PASJ'21)*, Takasaki (Online meeting), Japan, Aug. 2021, pp. 432–435 (in Japanese).

[15] K. Tamura *et al.*, "Status of SPring-8-II Vacuum System Design", presented at the 21st Annual Meeting of Particle Accelerator Society of Japan (PASJ'24), Yamagata, Japan, Jul. 2024, THP075, unpublished (in Japanese).

[16] M. Masaki *et al.*, "Design Optimization of Button-Type BPM Electrode for the SPring-8 Upgrade", in *Proc. 5th Int. Beam Instrumentation Conf. (IBIC'16)*, Barcelona, Spain, Sep. 2016, pp. 360–363. doi://10.18429/JACoW-IBIC2016-TUPG18

[17] T. Fujita *et al.*, "Long-term Stability of the Beam Position Monitors at SPring-8", in *Proc. 4th Int. Beam Instrumentation Conf. (IBIC'15)*, Melbourne, Australia, Sep. 2015, pp. 359–363. doi://10.18429/JACoW-IBIC2015-TUPB020

[18] H. Maesaka *et al.*, "Development of Beam Position Monitor for the SPring-8 Upgrade", in *Proc. 7th Int. Beam Instrumentation Conf. (IBIC'18)*, Shanghai, China, Sep. 2018, pp. 204–207. doi://10.18429/JACoW-IBIC2018-TUOC04

[19] S. Suzuki *et al.*, "Thermal and Structural Analyses of Vacuum Components for SPring-8-II", presented at the 21st Annual Meeting of Particle Accelerator Society of Japan (PASJ'24), Yamagata, Japan, Jul. 2024, WEP083, unpublished (in Japanese).